CrossMark

ORIGINAL PAPER

Improving the mechanical, thermal and electrical properties of polyurethane- graphene oxide nanocomposites synthesized by in-situ polymerization of ester-based polyol with hexamethylene diisocyanate

Ramin Shamsi[1] · Mojtaba Koosha[2] · Mojtaba Mahyari[1]

Abstract Many polyols or diols have been used for the synthesis of polyurethanes (PU), however, to the best of our knowledge, PU-graphene oxide (GO) nanocomposites synthesized with ester-based polyols have been rarely studied. In this work ester-based polyol synthesized by the reaction of adipic acid and 1,4 butane diol, was in-situ polymerized with hexamethylene diisocyanate (HDI) and GO to prepare PU-GO nanocomposites. The content of GO was changed from 1 to 2.5 wt% and its effect on the mechanical, thermal and electrical properties of the samples were examined. The presence of GO more than 1.5% in the nanocomposites resulted in brittle samples and reduced the tensile strength, however, the Young's modulus of the samples containing 1 and 1.5% was increased to 11 and 12.08-fold (275 and 302 MPa) compared to the neat PU (25 MPa), respectively. The shore A hardness of the samples was increased from 86 for PU to 96 for PUGO-1.5. The abrasion resistance of the samples was decreased by increasing the GO content. Results of the thermogravimetric analysis showed that higher amounts of GO increase the thermal stability of the samples. The chemical and physical interactions between the surface of GO nanolayers and the PU chains were confirmed by FTIR spectroscopy. The dynamic mechanical analysis of the samples showed that GO nanolayers decreased the molecular motions of the PU chains in the nanocomposites which were noticed by shifting the glass transition to the higher temperatures.

Introduction

Graphene sheets have been emerged as the subject of enormous researches due to their exceptional electrical and mechanical properties [1]. Graphene has a high basal plane elastic modulus of about 1 TPa, ultimate tensile strength of 130 GPa and room temperature charge carrier mobility of 10,000 cm^2/Vs [2]. Though, the addition of small amounts of graphene can significantly alter the mechanical and electrical properties of polymers. Graphene layers can be produced by several methods such as mechanical cleavage [3], liquid phase exfoliation [4], chemical vapor deposition [5], etc., however, graphene sheets with high purity produced from these methods tend to roll back into nanotubes or stack into graphite so as to minimize their surface energy [6, 7]. New methods have been developed for the mass production of graphene layers from graphene oxide (GO) by covalent bonding of oxygen groups on the surface of the sheets which prevents re-stacking of the planar structures [5].

Polymer-GO nanocomposites can be produced by solution mixing, melt mixing or in-situ polymerization. Exfoliation of the GO into nanoplatelets is an important issue in the fabrication of polymer/GO nanocomposites. It has been shown that GO can form stable suspensions in polar aprotic solvents as

✉ Mojtaba Mahyari
  Mo.Mahyari@gmail.com

  Mojtaba Koosha
  mojtaba.koosha@gmail.com

[1] Elites Advanced Research Center, Malek-Ashtar University of Technology, P.O. Box, 16765-3454, Tehran, Iran

[2] Department of Pulp and Paper, Faculty of Energy and New Technologies, Zirab Campus, Shahid Beheshti University, Mazandaran, Iran

well as isocyanates [8], which enables the production of exfoliated GO/polymer nanocomposites by in-situ polymerization.

Polyurethane (PU) as a multi-block copolymer consists of alternating soft and hard segments. The hard segment is made from a diisocyanate and a chain extender and the soft segment consists of a polyether or polyester polyol. Thermodynamic incompatibility between hard and soft segments develops micro-phase separated PU morphologies [9]. Though, PUs can be tailored to match the desired application by carefully selecting the synthesis method, type of reactants and their ratios [10]. In our previous works, we have synthesized GO nanolayers and reported their applications in catalysis [11–13], biosensors [14, 15] and environmental monitoring [16].

In another work, adhesive PUs were synthesized based on the product obtained from aminolysis of PET waste, ether-type polyol, 1,4-butanediol and various molar ratios of hexamethylene diamine (HDI). The synthesized PUs were applied as adhesives on various substrates. A comparison of the maximum bond strength of the synthesized PU adhesive to that of commercial adhesives revealed a 2.2-fold increase [17]. We also synthesized novel biodegradable PUs using bis (2-hydroxy ethylene) terephthalamide (BHETA). At first, polyols with different molecular weights have been synthesized via ring opening polymerization of caprolactone by BHETA, and then urethane linkages were formed using HDI. Thermal, chemical, mechanical and dynamic mechanical properties, morphology, biodegradability, and UV resistance of the synthesized PUs have also been investigated [18].

In other works, we have synthesized novel polyester diol obtained from PET waste and used it in the synthesis of PU and PU nanocomposites [19, 20]. In another work, we synthesized ester-based polyols by the reaction of adipic acid with three commonly used diols and the resulting polyols were reacted with HDI to synthesize different PU samples [21]. The effect of the type of ester-based polyols, the molar ratio of the hard to soft segment and type of diisocyanate, on the mechanical and thermal properties of PU nanocomposites was considered. We showed that the PU sample polymerized by the reaction of HDI with the ester-based polyol synthesized by the reaction of adipic acid and 1,4-butane diol, was the optimum sample regarding its mechanical and thermal properties. We also investigated the effect of carbon nanotubes (CNT) on the mechanical, thermal and electrical properties of PU-CNT nanocomposites.

Recently, PU-GO nanocomposites have been the subject of many researches [22–25]. It is shown that the addition of only 1% GO during polymerization of PU can significantly enhance the mechanical and electrical properties of PU nanocomposites [26]. Different diols and diisocyanates have been used for in-situ polymerization of PU-GO nanocomposites. To the best of our knowledge, PU-GO nanocomposites, in-situ polymerized with an ester-based polyol and HDI has not been studied in the previous works. The aim of this paper is to study the effect of GO content on the mechanical, thermal and electrical properties of PU-GO nanocomposites. In-situ polymerized nanocomposite samples were prepared and characterized by Fourier transform infrared spectroscopy (FTIR), dynamic mechanical analysis (DMA), tensile strength, thermogravimetric analysis (TGA) and electrical conductivity measurements.

Materials and methods

Materials

Ethylene glycol, 1,4-butane diol (BD), zinc acetate dihydrate (ZA), adipic acid (AA), dibutyltin dilaurate (DBTDL), hexamethylene diamine (HDI), dimethyl formamide (DMF), pyridine, phenolphthalein, NaOH and acetic anhydride were purchased from Merck (Germany). 2-methyl 1,3 propane diol was obtained from Aldrich. Silicon oil was used as media for heating. GO was synthesized according to the Hummer's method as reported in our previous paper [12].

Synthesis of the ester-based polyol (polyol-BD)

Ester-based polyol was synthesized by reaction of BD and AA. In a four necked glass reactor, AA and BD were charged with a mole ratio of BD: AA (1.8:1) and ZA (1 wt% of BD) as a catalyst. The reactor was purged with nitrogen gas and the other necks were filled with a condenser and a thermometer. The system was placed in a silicon oil bath on a magnetic stirrer, the temperature was maintained at 140 °C for 2 h and then increased to 210 °C for 2 h. H_2O vapors as the byproduct of the reaction were removed from the system by a vacuum pump. The final product of this step was used as Polyol-BD for the rest of synthesis.

Characterization of polyol-BD

The hydroxyl number (HN) and acid number (AN) of Polyol-BD were determined according to the standard NFT 52–113. In brief, 0.5 g of Polyol-BD was charged in a 50 ml round bottom flask equipped with a condenser, placed over a magnetic stirrer and mixed with 20 ml acetylate solution (containing pyridine: acetic anhydride 1000:127, v:v). The mixture was heated to 100 °C for 2 h then cooled to room temperature and titrated with NaOH 0.5 M and phenolphthalein. The same procedure was performed with a control solution.

The synthesized Polyol-BD was characterized by FTIR, nuclear magnetic resonance (NMR) and gel permeation chromatography (GPC).

FTIR spectra of the Polyol-BD was recorded with the BOMEM SRG 1100G instrument. ^{1}H–NMR spectra were

measured on a Bruker NMR spectrometer (250 MHz) in CDCl₃.

GPC measurement was performed on a Waters 510 Instrument equipped with Shodex GPC KF-800 series columns kept at 35 °C. The eluent was chloroform, with a flow of 1 ml.min⁻¹.

Synthesis of nanocomposites by in-situ polymerization

Different solutions containing Polyol-BD, DBTDL (1 wt% per weight of Polyol-BD) as catalyst and GO (1, 1.5, 2 and 2.5 wt%) were prepared in DMF and sonicated by commercial probe sonicator (QSonica Q700, LLC, USA) with an adjustable amplitude 20% and a power of 300 W for 20 min and immediately charged into a three necked flask equipped with a condenser and thermometer under nitrogen purge. The temperature was increased to 40 °C, then HDI solution in DMF (molar ratio HDI:Polyol-BD 3:2) was added to the reactor drop-wise and the temperature was increased to 80 °C for 2 h. BD solution in DMF (molar ratio HDI:BD 3:1) was added to the flask and the reaction was continued for 3 min. At last, the reactants were charged into rectangular and Dumbbell-shaped molds preheated to 50 °C, placed in an oven at 80 °C for 10 h to complete the reactions and used for the rest of characterization tests.

Characterization of the nanocomposites

Attenuated total reflectance-Fourier transform infrared spectroscopy (ATR-FTIR)

The ATR-FTIR analysis was performed on the surface of the prepared nanocomposites with a Bruker Equinox 55 FTIR spectrometer in reflection mode. The spectra of the nanocomposites were achieved by 20 scans in the wavenumber range 400–4000 cm⁻¹ with a resolution of 2 cm⁻¹.

Morphology

The morphology of the synthesized GO was observed by Transmission electron microscopy (TEM, model EM10C, Zeiss, Germany) and field emission scanning electron microscopy (FE-SEM, model S-4160, Hitachi, Japan). The morphology of PU, PUGO-1 and PUGO-2 nanocomposite samples were observed by SEM (model AIS-2100, Seron Technology, Korea). The nanocomposite samples were broken in liquid nitrogen and the fracture surface was coated with Au and used for SEM.

Tensile strength

The Dumbbell-shaped nanocomposite samples were tested according to ASTM D 1638 with a Cesare Galdabini SPA

tensile tester at the extension rate of 50 mm/min. The elastic modulus (E), ultimate tensile strength (UTS) and elongation at break (ε_b) were calculated and reported by the machine software. A number of 4 replicates were tested and the data were reported as an average ± standard deviation.

Hardness

Shore A hardness of nanocomposite samples were measured with Prüfen Messen tester according to the DIN 53505 standard test method.

Abrasion resistance

The abrasion resistance of the nanocomposites was measured by Prüfen Messen tester according to the standard GB/T 9867–1998. The samples were cut into disks with 13 mm diameter and tested under the applied force of 10 N with a rubbing distance of 40 m on the surface of the roll. The weight loss of each sample was calculated by the difference in weight before and after the abrasion test and reported as abrasion resistance with the units of mg.

Dynamic mechanical thermal analysis (DMTA)

The samples were prepared in rectangular shaped molds with dimensions of 1× 3 cm and thickness of 0.25 mm for the DMTA test. The experiments were performed in tension mode utilizing a TTDMA dynamic mechanical analyzer (Triton Technology Incorporation). The samples were fixed between the static and movable clamps with a free length of about of 5 mm. Dynamic strain amplitude (displacement) of 0.007 mm and the frequency of 1 Hz was selected to be in the linear
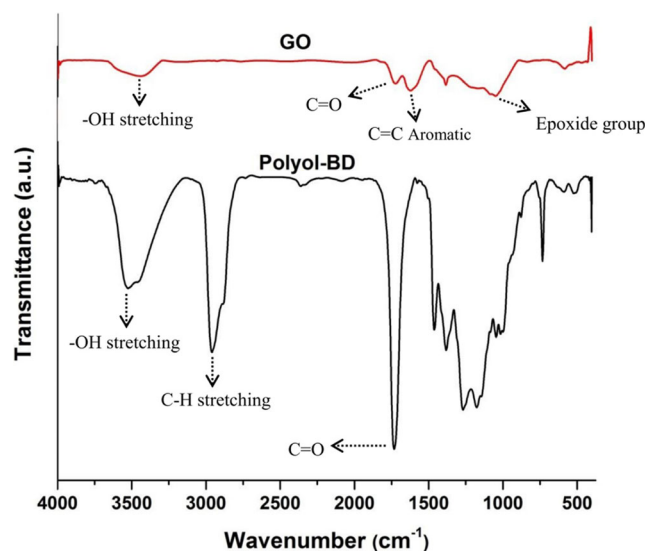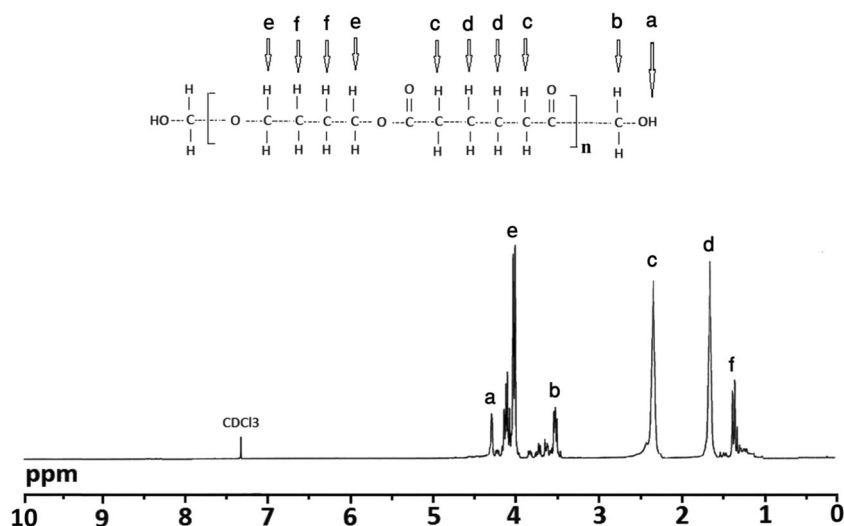

Fig. 1 FTIR spectrum of the synthesized GO and Polyol-BD

Fig. 2 Chemical structure and ^{1}H–NMR spectrum of Polyol-BD

viscoelastic region. The temperature sweep was applied to the samples from −100 °C to 150 °C with a heating rate of 3 °C/min. Storage modulus (E′), loss modulus (E″) and damping (tan δ) of the samples were reported in the temperature range of the test.

Thermogravimetric analysis (TGA)

TGA curves for the nanocomposite samples were recorded by a Mettler Toledo analyzer from room temperature to 600 °C at the heating rate of 10 °C/min.

Electrical conductivity

The electrical conductivity of the nanocomposite samples was measured using PGSTAT 302 N tester machine.

Results

Synthesis and characterization of polyol-BD

Polyol-BD was synthesized by the step polymerization reaction between BD and AA. FTIR spectrum of Polyol-BD is displayed in Fig. 1. A strong and broad peak at 3530 cm^{-1} was due to the O-H stretching of hydroxyl groups in the chemical structure of Polyol-BD. Peaks at 2880 and 2960 cm^{-1} can

be related to symmetric and asymmetric C-H stretching, respectively. The peak observed at 1700 cm^{-1} was ascribed to the formation of ester bonds formed by the reaction of AA and BD.

Here, the ^{1}H–NMR technique was used for detailed characterization of the chemical structure and also, determination of the number average molecular weight ($\overline{M}_n$) [18, 19]. The ^{1}H–NMR spectrum and the chemical structure of synthesized Polyol-BD are presented in Fig.2. The peak assignment is as follows: *(a)* δ: 4.3 ppm (hydroxyl protons of Polyol-BD); *(b)* δ: 3.5 ppm (−CH$_2$- protons in the vicinity of hydroxyl groups); *(c)* δ: 2.2–2.4 ppm (−CH$_2$- protons related to adipic acid section in α-position to -C = O); *(d)* δ: 1.5–1.7 ppm (−CH$_2$- protons related to adipic acid section in β-position to -C = O); *(e)* δ: 3.9–4.2 ppm (−CH$_2$- protons related to butane diol section in α-position to -O-C = O); *(f)* δ: 1.1–1.4 ppm (−CH$_2$- protons related to butane diol section in β-position to -O-C = O). The presence of ester linkages in the chemical structure of the polyol repeat units were also confirmed by the ^{1}H–NMR spectroscopy. The number average molecular weight of Polyol-BD ($\overline{M}_n$) was determined by ^{1}H–NMR using the following equation (Eq. 1):

$$\overline{M}_n = 22\,(\delta_{BD}/\delta_{OH}) + 28\,(\delta_{AA}/\delta_{OH}) + 62 \qquad (1)$$

δ_{BD}: Peak area of total protons of CH$_2$ related to butane diol section which were assigned to (e) and (f) in Fig. 2

Table 1   Calculated $\overline{M}_n$ values by using ^{1}H–NMR, titration and GPC techniques

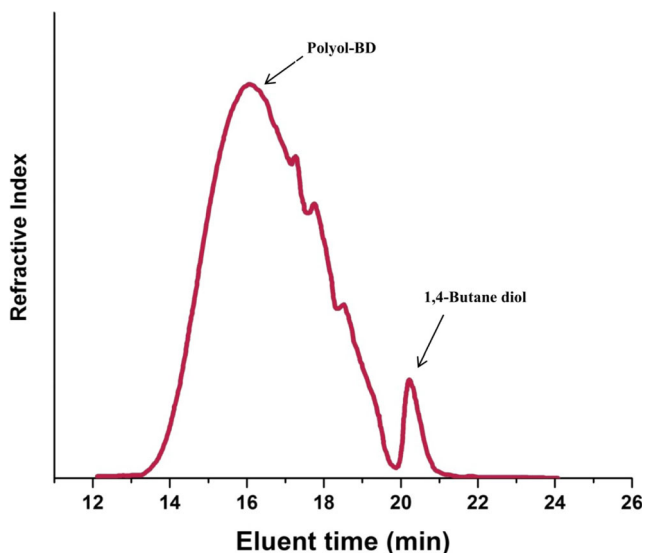| Sample Code	M_n Determined by ^{1}HNMR techniques	M_n Determined by titration	M_n Determined by GPC techniques
Polyol-BD	2240	2210	2130

Fig. 3 GPC chromatogram of Polyol-BD

δ_{AA}: Peak area of total protons of CH_2 related to adipic acid section which were assigned to (c) and (d) in Fig. 2

δ_{OH}: Peak area of total protons of -OH which were assigned to (a) in Fig. 2

As an outcome, the number average molecular weight of Polyol-BD was calculated to be 2240 g/mol (Table 1).

Also, based on the following equation (Eq. 2) and having hydroxyl number (HN = 46.45) and acid number (AN = 4.33), $\overline{M}_n$ was determined to be 2210 for Polyol-BD by using titration method (Table 1).

$$\overline{M}_n = \frac{56100*\overline{f}}{HN + AN} \xrightarrow{f=2} \overline{M}_n = \frac{112220}{HN + AN} \qquad (2)$$

To further confirm the molecular weight of Polyol-BD, it was also determined by GPC and the results are reported in Fig. 3 and Table 1. According to Table 1, it is notable that the number average molecular weight obtained from GPC is in consistence with the data calculated from ^1H–NMR and titration techniques.

Table 2 Major FTIR peaks and the relevant functional groups of the synthesized GO

Chemical group	Wavenumber (cm^{-1})
-OH	3440
C-H stretching	2960, 2927
C = O	1720
C = C Aromatic	1620
C-H deformation	1380
C-OH bending	1170,1216
C-O	1080
Epoxide group	1040

Synthesis and characterization of PU and PU/GO nanocomposites

In this work PU-GO nanocomposites were synthesized by the reaction of an ester-based polyol (Polyol-BD), HDI and BD as the chain extender in the presence of GO nanolayers. The content of GO in the nanocomposites was increased from 1 to 2.5 wt.% and its effect on the chemical structure, mechanical, thermal and electrical properties was investigated.

Chemical analysis

The FTIR spectroscopy was used to study the chemical structure of the nanocomposites. The FTIR spectrum for pristine GO is shown in Fig.1 and the peaks for major functional groups of GO are listed in Table 2. The strong absorption band at 3440 cm^{-1} is due to OH groups present on the surface of GO. The peak for the carbonyl group was appeared at 1720 cm^{-1}. The bands at 1080 cm^{-1} and 1040 cm^{-1} were due to the presence of epoxide groups. The mentioned peaks approve the presence of carbonyl, hydroxyl and epoxide groups in the structure of GO nanolayers, in agreement with the literature data [22].

The FTIR spectra for the synthesized PU and PU-GO nanocomposites are presented in Fig. 4. The analysis of the NH and C = O stretching vibrations gives valuable information about any possible interactions between PU chains with GO in the PU nanocomposites. It was observed that by increasing the GO content from 1 to 2.5%, the characteristic peaks of PU (peaks at about 3300 cm^{-1} related to NH stretching vibrations and about 1720 cm^{-1} due to C = O stretching) were shifted to lower frequencies which indicate the enhancement of the
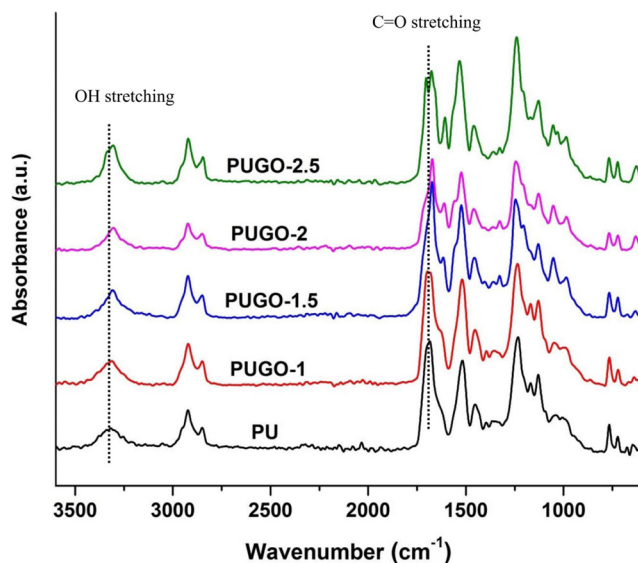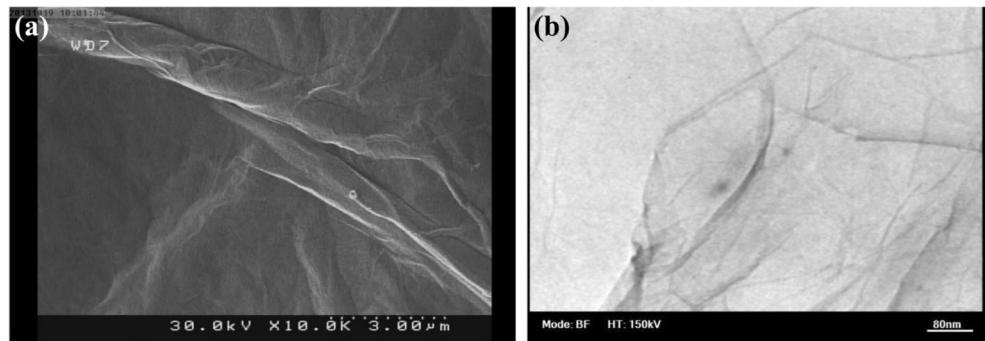

Fig. 4 FTIR spectra of the in-situ polymerized PU-GO nanocomposites

Fig. 5 Morphology of GO nanolayers: **a** SEM and **b** TEM image

hydrogen bonding interactions between the GO nanolayers and urethane groups present in the PU chains.

In GO based PU composites, there is a possibility for the formation of hydrogen bonds between PU and GO nanolayers. The NH and C = O groups from a PU hard segment can donate electron pairs, whereas proton of -OH and -COOH groups residing on the surface of GO can act as one of the acceptor groups. Here, increasing the amount of GO caused to the formation of higher hydrogen bonds between PU chains and functional groups of GO resulting in a chemical shift to lower wavenumbers.

Morphology

The morphology of the synthesized GO is presented in Fig. 5a (SEM) and Fig. 5b (TEM). Figure 5b displays the thin membrane morphology for the synthesized GO.

Figure 6 shows the SEM image of the synthesized PU (Fig. 6a) as well as the nanocomposite samples PUGO-1 (Fig. 6b) and PUGO-2 (Fig. 6c). From Fig. 6b it can be seen that the GO sheets are embedded and well dispersed within the PU matrix. Interestingly, GO sheets in the PU matrix appear to be extended and interconnected due to the chemical affinity with the matrix. Comparing the morphology of PUGO-1 and PUGO-2, larger agglomerations are observed for the PUGO-2 while the better dispersion of GO nanolayers in the matrix can be seen for the PUGO-1. In the SEM image for the PUGO-1 (Fig. 6b), a strong interface merged to the PU matrix is detected, however, the morphology of the interface for the PUGO-2 (Fig. 6c) is distinct which indicates weak interface and interaction with the matrix. It is notable that many OH and COOH groups are present at the surface of GO which interacts with the urethane and carbonyl groups of PU chains through hydrogen bonding. In the SEM image for the PUGO-1, we

Fig. 6 The morphology of the samples: SEM images for **a** PU, **b** PUGO-1 and **c** PUGO-2
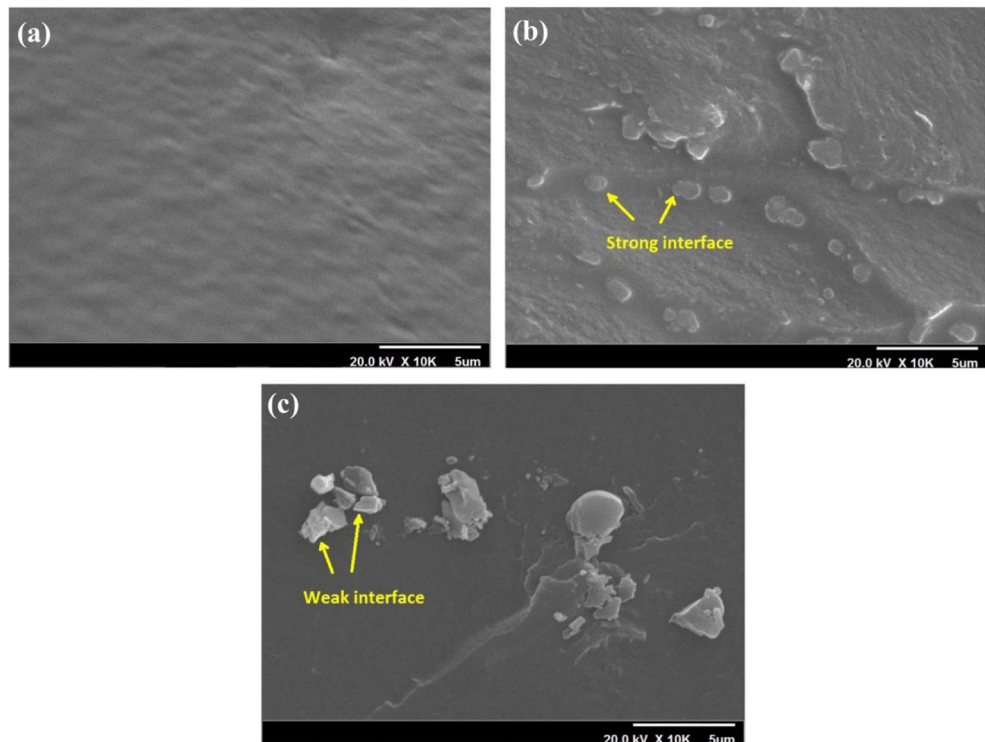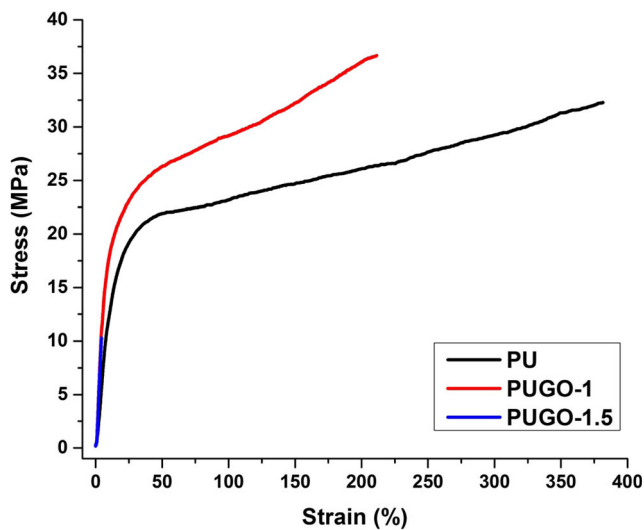
Fig. 7 Stress-strain curves of PU, PUGO-1 and PUGO-1.5 samples at the extension rate of 50 mm/min

observed a better dispersion of GO nanolayers, though, a higher surface area exists between the surface of GO and PU chains. In contrast, the agglomerated morphology observed for PUGO-2, reduces the effective surface area for the interactions.

Mechanical properties

The stress-strain curves and the results of the mechanical properties of the samples are presented in Fig. 7 and Table 3, respectively. Due to the presence of a high number of functional groups on the surface of GO (carboxylic acids, hydroxyl and epoxy), significant chemical and physical interactions occurs between hydroxyl and carboxylic acid groups on the surface of GO and urethane groups of PU chains during in situ-polymerization. These interactions reduce the mobility of polymer chains and increase the modulus of the samples [24, 27, 28]. Therefore, as can be seen from the data of Table 3, the Young's modulus of the samples was increased by increasing the GO content. In the case of the samples PUGO-2 and

PUGO-2.5, the tensile test was not performed because the samples were very brittle. The high number of functional groups due to the strong chemical and physical interactions between the GO nanolayers and PU chains highly reduces the chain mobility resulting in the brittleness of the samples PUGO-2 and PUGO-2.5.

Hence, from the tensile strength data, we observed an increase in the elastic modulus and hardness, reduction of the strength, elongation at break and the abrasion resistance of the samples by increasing the GO content. These results are in agreement with the morphology images of the samples presented in Fig. 6. By increasing the GO content in the nanocomposites, agglomerated morphology reduces the favorable interactions.

Dynamic mechanical analysis

Dynamic mechanical tests can provide valuable data about the viscoelastic behavior and thermal transitions inside polymers. Figure 8 presents the storage modulus and damping behavior of PU-GO nanocomposites in the temperature range of −100 to 150 °C at constant frequency of 1 Hz. In agreement with the Young's modulus of the samples, the storage modulus was increased with increasing the GO content. Due to the planar structure and high number of functional groups on the surface of GO, the reduction of chain mobility was evident from Fig. 8 in which the damping was reduced and the temperature of maximum tan δ was shifted to higher temperatures. Table 4 lists the temperature of the maximum damping and loss modulus (the loss modulus curves were not shown in Fig.8) which is assumed as the glass transition temperature (T_g) of the samples. The glass transition temperature was increased from −18 °C for the PU sample to 3.8 °C for PUGO-1 and 10.3 °C for PUGO-1.5 which indicates the physical and chemical interactions between the GO nanolayers and the PU chains. Due to the high stiffness of the GO nanolayers, their interaction with PU chains restricts their segmental and frictional motions resulting in higher glass transition temperatures for the PU-GO nanocomposites.

Table 3 The tensile properties, hardness and abrasion resistance of the PU and PU-GO nanocomposite samples

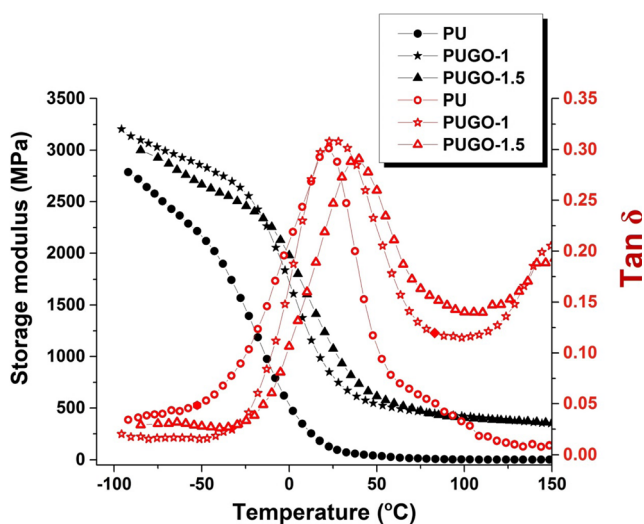| Sample	Strain (%)	Tensile strength (MPa)	Young's modulus (MPa)	Hardness (shore A)	Mass Loss on Abrasion (mg)
PU	404 ± 21	45 ± 3.8	25 ± 1.5	86 ± 0.4	46 ± 5
PUGO-1	210 ± 16	36 ± 2.1	275 ± 11	89 ± 0.2	112 ± 13
PUGO-1.5	10.3 ± 3	4.4 ± 0.8	302 ± 7	96 ± 1.8	Low resistance to abrasion
PUGO-2		Brittle		99 ± 0.7	Low resistance to abrasion
PUGO-2.5		Brittle		99 ± 0.6	Low resistance to abrasion

Fig. 8 Dynamic mechanical properties of PU, PUGO-1 and PUGO-1.5 samples at constant frequency of 1 Hz

TGA results

Thermal degradation of the samples was investigated by TGA test. Table 5 shows the temperatures of 10, 50 and 90% mass loss as well as the residual char for PU and PU-GO nanocomposites. TGA curves for PU and PU-GO nanocomposites are presented in Fig. 9. All samples showed a two-step degradation pattern: the first stage attributed to the degradation of hard segments and the second stage due to the degradation of soft segments [29, 30]. The thermal degradation of PU and PU-GO nanocomposites were similar, but it was observed that thermal stability of PU-GO nanocomposites was increased with higher amounts of GO. The reasons for this observation will be discussed later.

Electrical properties

The effect of GO on the electrical conductivity of PU-GO nanocomposites is presented in Fig. 10. As shown, it can be seen that the electrical conductivity of the nanocomposites was increased by increasing the GO content in PU matrix. The conjugating π bonds and bonding between GO nanolayers and PU matrix increases the electrical conductivity.

Discussion

In this paper, we considered the effect of GO nanolayers on the mechanical, thermal and electrical properties of in-situ polymerized PU-GO nanocomposites. In PU synthesis, the selection of diisocyanate and polyol is very important to achieve suitable mechanical and thermal properties. In our previous study, different combinations of diisocyanates and synthesized ester-based polyols were used as monomers for the polymerization of PU samples and the mechanical and thermal properties of the samples were measured [21]. We found that the PU sample prepared by the reaction of Polyol-BD with HDI has the best mechanical and thermal properties. Then, we prepared in-situ polymerized PU-CNT nanocomposites and measured the mechanical, thermal and electrical properties of the samples. In this work, we prepared and characterized in-situ polymerized PU-GO nanocomposites. The effect of GO and CNT nanofillers on the mechanical and thermal properties of the nanocomposites are different due to their structure and interactions with polymer chains. GO nanolayers highly increase the Young's modulus due to their planar and stiff structure, however, the effect of CNT on the Young's modulus is lower because it has a more flexible structure. To prove this, we compared the Young's modulus of the nanocomposite samples in this work and in the previous work. The Young's modulus for PUCNT-1 containing 1% CNT was 90 MPa while the Young's modulus for the PUGO-1 was 275 MPa. We achieved a Young's modulus of 188 for the PUCNT-2.5 while the sample PUGO-2.5 was not measureable. These data showed that presence of small amounts of GO can highly increase the Young's modulus of the nanocomposites compared to the CNT. This result also proves the higher load transfer efficiency of GO nanolayers compared to the CNTs.

Pokharel and coworkers investigated the effect of hard segment length on the thermal and mechanical properties of in-situ polymerized PU-GO nanocomposites [23]. They achieved a 4.8-fold increase in Young's modulus and 6.8-fold increase in tensile strength by addition of 4% GO, without sacrificing the elongation at break. In this work, we achieved a 12-fold increase in the Young's modulus by incorporation of 1% GO which was higher than the previous reports [2, 23, 31, 32].

Table 4 The glass transition temperature (T_g) and temperature of maximum damping of the PU, PUGO-1 and PUGO-1.5

Sample	Glass transition temperature (T_g)[a]	Temperature of maximum damping
PU	-18	23
PUGO-1	3.8	25.4
PUGO-1.5	10.3	39.7

[a] Obtained from loss modulus-temperature (E"-T) curve peak

Table 5 The temperatures of 10%, 50% and 90% mass loss and the mass % of ash remained at 600 °C for the PU and PU-GO nanocomposites

Sample code	$T_{10\%}$	$T_{50\%}$	$T_{90\%}$	Mass % of ash remained at 600 °C
PU	283	332	442	3.5
PUGO-1	296	341	460	3.95
PUGO-1.5	307	350	480	5.1
PUGO-2	318	368	486	5.95
PUGO-2.5	315	367	497	7.2

In this work, the strength of nanocomposite samples was reduced by incorporation of GO. This was due to the strong chemical and physical interactions between the GO nanolayers and PU chains which reduced the chain mobility and decreased the strength. In the work of Pokharel et al. the strength of the neat PU was about 6.1 MPa and it was increased to 41.8 MPa after incorporation of 4% GO. However, the strength of our neat PU was 45 MPa which was greater than the neat PU used in the work of Pokharel et al. Although, the strength was reduced by increasing the GO content in the nanocomposites, we had high strength values in our study compared to the other data reported in the literature [2, 31–33]. This result was related to the chemical structure of the ester-based polyol which was synthesized and used in this study.

The higher thermal stabilization of PU-GO nanocomposites compared to the neat PU could be attributed to the 2-dimensional planar structure of the dispersed GO in the PU matrix. As well, the GO can play a barrier role for preventing speedy removal of degradation products from the underlying
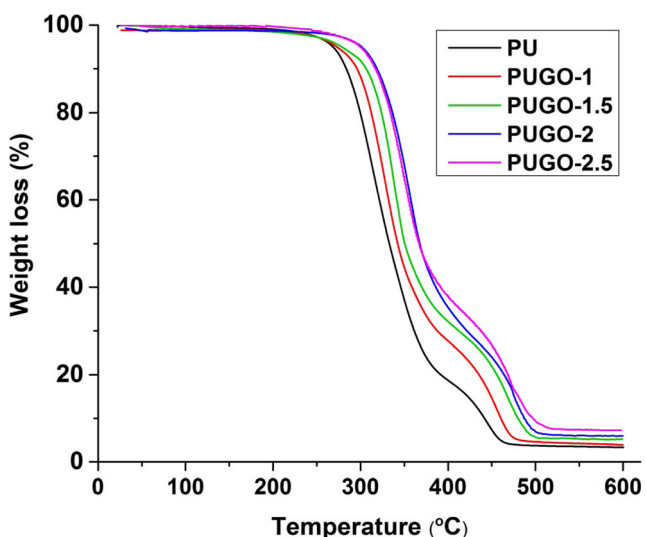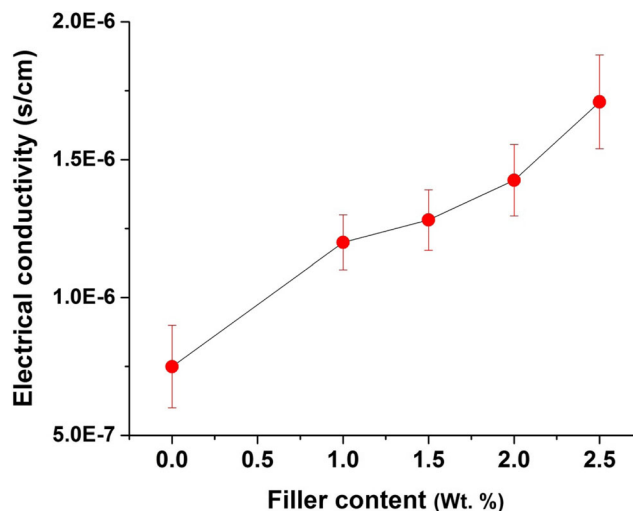

Fig. 10 Changes in the electrical conductivity of the in-situ polymerized PU and PU-GO nanocomposites by the weight fraction of GO

PU matrix thus, retarding the process of degradation [34]. As it became clear according to the ATR-FTIR results, the good interfacial interactions between urethane groups in the PU with the functional groups present on the GO surface, can be another reason for the improvement of the thermal stability in PU-GO nanocomposites. These interfacial interactions (covalent and non-covalent) decrease the PU-GO thermal boundary resistance and results in the easy transfer of heat from the PU matrix to the GO. Therefore, heat distribution throughout the nanocomposites can be performed without the creation of any "hot spots", a characteristic which causes to lower thermal decomposition temperatures [35, 36].

Comparing the TGA results for PU-CNT nanocomposites from our previous work, with the TGA results for the currently studied samples, it is notable that the thermal stability of the PU-GO nanocomposites was higher (about 10 °C) than the PU-CNT nanocomposites. Thus, it can be concluded that the barrier role and heat distribution by GO in the PU matrix is better compared to the CNTs because of the 2-dimensional planar structure of the GO and also, good interactions with the urethane groups.

Conclusion

In this work, the ester-based Polyol-BD was synthesized and its number average molecular weight was determined using ^{1}H–NMR, titration and GPC techniques. The obtained $\overline{M}_n$ values from these three techniques were in good accordance. The synthesized Polyol-BD was used for in-situ polymerization of HDI in the presence of GO. The resulting neat PU showed a high Young's modulus and tensile strength compared to the previous works. Also, the Young's modulus of the PUGO-1 nanocomposite samples increased a 12-fold

Fig. 9 Results of TGA analysis for the in-situ polymerized PU and PU-GO nanocomposites at the heating rate of 10 °C/min

compared to the neat PU, due to the strong chemical and physical interactions between PU chains and GO nanolayers, however, the tensile strength was reduced by increasing the GO content. PU-GO nanocomposites showed enhanced thermal properties and higher T_g, storage and loss modulus compared to the neat PU. The electrical conductivity of the PUGO nanocomposites was also increased.

References

1. Kim H, Abdala AA, Macosko CW (2010) Graphene/polymer nanocomposites. Macromolecules 43(16):6515–6530

2. Kim H, Miura Y, Macosko CW (2010) Graphene/polyurethane nanocomposites for improved gas barrier and electrical conductivity. Chem Mater 22(11):3441–3450

3. Novoselov KS, Geim AK, Morozov SV, Jiang D, Zhang Y, Dubonos SV, Grigorieva IV, Firsov AA (2004) Electric field effect in atomically thin carbon films. Science 306(5696):666–669

4. Hernandez Y, Nicolosi V, Lotya M, Blighe FM, Sun Z, De S, McGovern I, Holland B, Byrne M, Gun'Ko YK (2008) High-yield production of graphene by liquid-phase exfoliation of graphite. Nat Nanotechnol 3(9):563–568

5. Park S, Ruoff RS (2009) Chemical methods for the production of graphenes. Nat Nanotechnol 4(4):217–224

6. Viculis LM, Mack JJ, Kaner RB (2003) A chemical route to carbon nanoscrolls. Science 299(5611):1361–1361

7. Li Q, Li Z, Chen M, Fang Y (2009) Real-time study of graphene's phase transition in polymer matrices. Nano Lett 9(5):2129–2132

8. Stankovich S, Piner RD, Nguyen ST, Ruoff RS (2006) Synthesis and exfoliation of isocyanate-treated graphene oxide nanoplatelets. Carbon 44(15):3342–3347

9. Chattopadhyay D, Raju K (2007) Structural engineering of polyurethane coatings for high performance applications. Prog Polym Sci 32(3):352–418

10. Delebecq E, Pascault J-P, Boutevin B, Fo G (2012) On the versatility of urethane/urea bonds: reversibility, blocked isocyanate, and non-isocyanate polyurethane. Chem Rev 113(1):80–118

11. Mahyari M, Shaabani A, Bide Y (2013) Gold nanoparticles supported on supramolecular ionic liquid grafted graphene: a bifunctional catalyst for the selective aerobic oxidation of alcohols. RSC Adv 3(44):22509–22517

12. Mahyari M, Shaabani A (2014) Graphene oxide-iron phthalocyanine catalyzed aerobic oxidation of alcohols. Appl Catal A Gen 469:524–531. doi:10.1016/j.apcata.2013.09.024

13. Mahyari M, Laeini MS, Shaabani A, Kazerooni H (2015) Gold nanoparticles supported on three-dimensional nitrogen-doped graphene: an efficient catalyst for selective aerobic oxidation of hydrocarbons under mild conditions. Appl Organomet Chem 29(7):456

14. Dehsari HS, Gavgani JN, Hasani A, Mahyari M, Shalamzari EK, Salehi A, Taromi FA (2015) Copper (ii) phthalocyanine supported on a three-dimensional nitrogen-doped graphene/PEDOT-PSS nanocomposite as a highly selective and sensitive sensor for ammonia detection at room temperature. RSC Adv 5(97):79729–79737

15. Hosseini H, Mahyari M, Bagheri A, Shaabani A (2014) A novel bioelectrochemical sensing platform based on covalently attachment of cobalt phthalocyanine to graphene oxide. Biosens Bioelectron 52:136–142

16. Behbahani M, Tapeh NAG, Mahyari M, Pourali AR, Amin BG, Shaabani A (2014) Monitoring of trace amounts of heavy metals in different food and water samples by flame atomic absorption spectrophotometer after preconcentration by amine-functionalized graphene nanosheet. Environ Monit Assess 186(11):7245–7257

17. Shamsi R, Abdouss M, Sadeghi GMM, Taromi FA (2009) Synthesis and characterization of novel polyurethanes based on aminolysis of poly (ethylene terephthalate) wastes, and evaluation of their thermal and mechanical properties. Polym Int 58(1):22–30

18. Sadeghi GMM, Shamsi R, Sayaf M (2011) From aminolysis product of PET waste to novel biodegradable polyurethanes. J Polym Environ 19(2):522–534

19. Shamsi R, Mir Mohamad Sadeghi G (2016) Novel polyester diol obtained from PET waste and its application in the synthesis of polyurethane and carbon nanotube-based composites: swelling behavior and characteristic properties. RSC Adv 6(44):38399–38415. doi:10.1039/C6RA04127B

20. Shamsi R, Mir Mohamad Sadeghi G, Asghari GH (2016) Dynamic mechanical analysis of polyurethanes and carbon nanotube based composites obtained from PET waste. Polym Compos. doi:10.1002/pc.24155

21. Shamsi R, Mahyari M, Koosha M (2016) Synthesis of CNT-polyurethane nanocomposites using ester-based polyols with different molecular structure: mechanical, thermal, and electrical properties. J Appl Polym Sci. doi:10.1002/app.44567

22. Li Y, Pan D, Chen S, Wang Q, Pan G, Wang T (2013) In situ polymerization and mechanical, thermal properties of polyurethane/graphene oxide/epoxy nanocomposites. Mater Des 47:850–856

23. Pokharel P, Choi S (2015) The effect of hard segment length on the thermal and mechanical properties of polyurethane/graphene oxide nanocomposites. Compos A: Appl Sci Manuf 69:168–177

24. Qian X, Song L, Tai Q, Hu Y, Yuen RK (2013) Graphite oxide/polyurea and graphene/polyurea nanocomposites: a comparative investigation on properties reinforcements and mechanism. Compos Sci Technol 74:228–234

25. Fahim IS, Mamdouh W, Salem HA (2013) A nanoscale investigation of mechanical, thermal stability and electrical conductivity properties of reinforced thermoplastic polyurethane/graphene nanocomposite. American Journal of Nanoscience and Nanotechnology 1(1):31–40

26. Yousefi N, Gudarzi MM, Zheng Q, Lin X, Shen X, Jia J, Sharif F, Kim J-K (2013) Highly aligned, ultralarge-size reduced graphene oxide/polyurethane nanocomposites: mechanical properties and moisture permeability. Compos A: Appl Sci Manuf 49:42–50

27. Li Z, Young RJ, Wang R, Yang F, Hao L, Jiao W, Liu W (2013) The role of functional groups on graphene oxide in epoxy nanocomposites. Polymer 54(21):5821–5829

28. Kuilla T, Bhadra S, Yao D, Kim NH, Bose S, Lee JH (2010) Recent advances in graphene based polymer composites. Prog Polym Sci 35(11):1350–1375

29. Kumar M, Chung JS, Kong B-S, Kim EJ, Hur SH (2013) Synthesis of graphene–polyurethane nanocomposite using highly functionalized graphene oxide as pseudo-crosslinker. Mater Lett 106:319–321

30. Petrović ZS, Zavargo Z, Flyn JH, Macknight WJ (1994) Thermal degradation of segmented polyurethanes. J Appl Polym Sci 51(6):1087–1095

31. Cai D, Yusoh K, Song M (2009) The mechanical properties and morphology of a graphite oxide nanoplatelet/polyurethane composite. Nanotechnology 20(8):085712

32. Pokharel P, Lee DS (2014) Thermal and mechanical properties of reduced graphene oxide/polyurethane nanocomposite. J Nanosci Nanotechnol 14(8):5718–5721

33. Pokharel P (2014) High performance polyurethane nanocomposite films prepared from a masterbatch of graphene oxide in polyether polyol. Chem Eng J 253:356–365

34. Kuila T, Bose S, Hong CE, Uddin ME, Khanra P, Kim NH, Lee JH (2011) Preparation of functionalized graphene/linear low density polyethylene composites by a solution mixing method. Carbon 49(3):1033–1037

35. Bian J, Lin HL, He FX, Wei XW, Chang I-T, Sancaktar E (2013) Fabrication of microwave exfoliated graphite oxide reinforced thermoplastic polyurethane nanocomposites: effects of filler on morphology, mechanical, thermal and conductive properties. Compos A: Appl Sci Manuf 47:72–82

36. Cai D, Jin J, Yusoh K, Rafiq R, Song M (2012) High performance polyurethane/functionalized graphene nanocomposites with improved mechanical and thermal properties. Compos Sci Technol 72(6):702–707